Atmos. Chem. Phys. Discuss., doi:10.5194/acp-2016-536, 2016
Manuscript under review for journal Atmos. Chem. Phys.
Published: 12 July 2016

Atmospheric Chemistry and Physics Discussions

Effects of daily meteorology on the interpretation of space-based remote sensing of NO_2

Joshua L. Laughner[1], Azimeh Zare[1], and Ronald C. Cohen[1,2]

[1]Department of Chemistry, University of California, Berkeley, Berkeley, CA, USA
[2]Department of Earth and Planetary Science, University of California, Berkeley, Berkeley, CA, USA

Correspondence to: R.C. Cohen (rccohen@berkeley.edu)

Atmos. Chem. Phys. Discuss., doi:10.5194/acp-2016-536, 2016
Manuscript under review for journal Atmos. Chem. Phys.
Published: 12 July 2016

Atmospheric Chemistry and Physics Discussions

Abstract. Retrievals of tropospheric NO_2 columns from UV/visible observations of reflected sunlight require a priori vertical profiles to account for the variation in sensitivity of the observations to NO_2 at different altitudes. These profiles vary in space and time but are usually approximated using models that do not resolve the full details of this variation. Currently, no operational retrieval simulates these a priori profiles at both high spatial and high temporal resolution. Here we examine the additional benefits of daily variations in a priori profiles for retrievals already simulating a priori NO_2 profiles at sufficiently high spatial resolution to identify variations of NO_2 within urban and power plant plumes. We show the effects of introducing daily variation into a priori profiles can be as large as 40% and 3×10^{15} molec. cm^{-2} for an individual day and lead to corrections as large as 10% for a monthly average in a case study of Atlanta, GA. Comparing an optimized retrieval to a more standard one, we find that NO_x emissions estimated from space-based remote sensing can increase by $\sim 100\%$ when daily variations in plume location and shape are accounted for in the retrieval.

1 Introduction

NO_x (= NO + NO_2) is an atmospheric trace gas family that plays an important role in regulating the production of O_3 and particulate matter. NO_x is emitted into the atmosphere by natural processes (e.g. lightning, biomass burning) and anthropogenic sources, notably combustion. Understanding the contribution of each source is vital to determining the effectiveness of current and future efforts to improve air quality and to understanding the chemistry of the atmosphere. A substantial number of studies have utilized satellite observations to constrain NO_x emissions from lightning (e.g. Miyazaki et al. 2014; Beirle et al. 2010; Martin et al. 2007; Schumann and Huntrieser 2007), biomass burning (e.g. Castellanos et al. 2014; Mebust and Cohen 2014, 2013; Miyazaki et al. 2012; Mebust et al. 2011), anthropogenic NO_x emissions and trends (Ding et al., 2015; Lamsal et al., 2015; Tong et al., 2015; Huang et al., 2014; Gu et al., 2013; Miyazaki et al., 2012; Russell et al., 2012; Lin et al., 2010; Kim et al., 2009), and NO_x lifetime (Lu et al., 2015; de Foy et al., 2014; Valin et al., 2013).

The process of retrieving a troposphere NO_2 column from satellite observations requires three main steps. First, the raw radiances are fit using Differential Optical Absorption Spectroscopy (DOAS) to yield slant column densities (Richter and Wagner, 2011). Then, the stratospheric NO_2 signal must be removed (Boersma et al., 2011; Bucsela et al., 2013). Finally, the tropospheric slant column density (SCD) must be converted to a vertical column density (VCD) by use of an air mass factor (AMF) and Eq. (1). The AMF must account for the varying sensitivity of the satellite to NO_2 at different altitudes, and therefore a priori knowledge of that sensitivity and the vertical profile of NO_2 is required. Because the satellite is less sensitive to NO_2 near the surface, the AMF should be smaller in locations influenced by surface NO_x sources.

$$\mathrm{VCD} = \frac{\mathrm{SCD}}{\mathrm{AMF}} \tag{1}$$

A priori NO_2 profiles are generated using chemical transport models. Previous studies (e.g. Cohan et al. 2006, Wild and Prather 2006, Valin et al. 2011, Schaap et al. 2015) have demonstrated these modeled NO_2 profiles are strongly dependent on the spatial resolution of the chemical transport model used. The impact of model spatial resolution on satellite retrievals has

Atmos. Chem. Phys. Discuss., doi:10.5194/acp-2016-536, 2016
Manuscript under review for journal Atmos. Chem. Phys.
Published: 12 July 2016

Atmospheric Chemistry and Physics Discussions

been evaluated through case studies (Valin et al., 2011; Heckel et al., 2011; Yamaji et al., 2014) and through what could be termed "regional" retrievals (Russell et al., 2011; McLinden et al., 2014; Kuhlmann et al., 2015; Lin et al., 2015) that trade global coverage for improved spatial resolution of the input assumptions. These studies recommend model resolution of < 20 km to accurately capture NO_x chemistry on a priori profiles. Russell et al. (2011) showed that increasing the spatial resolution of the input NO_2 profiles produces a retrieval that better retrieves the spatial features of NO_2 plumes, reducing systematic bias by as much as 30%. Reducing these biases improves the clarity of the observed urban-rural gradients by providing unique urban and rural profiles, rather than one that averages over both types of locations. McLinden et al. (2014) showed that using 15 km resolution profiles was necessary to distinguish the NO_2 signal of the Canadian oil sands from the background.

Currently, only the Hong Kong-OMI retrieval has made use of daily a priori NO_2 profiles at < 20 km spatial resolution (Kuhlmann et al., 2015), covering the Pearl River Delta for the period October 2006 to January 2007. No operational retrieval covering the majority of the OMI data record does so. The current generation BEHR (Russell et al., 2011, 2012) and OMI-EC (McLinden et al., 2014) retrievals simulate monthly average NO_2 profiles at 12 and 15 km, respectively. Conversely, the DOMINOv2 (Boersma et al., 2011) and POMINO (Lin et al., 2015) retrievals simulate daily profiles at $2° \times 3°$ and $0.5° \times 0.667°$, respectively, which is insufficient to capture the full spatial variability of NO_2 plumes, but does capture large scale variations in meteorology. Lamsal et al. (2014) quantitatively compared NO_2 average profile shapes measured from the P3-B aircraft for each of six sites in the DISCOVER-AQ Baltimore/DC campaign with the modeled profile shape from the GMI chemical transport model used to compute the NO_2 a priori profiles in the NASA OMNO2 retrieval, which uses monthly average NO_2 profiles at $2° \times 2.5°$ spatial resolution. They found up to 30% differences between the measured and modeled profile shape factors (i.e. $S(p)$ in Eq. 3) at any single pressure throughout the troposphere. Several sites (Edgewood, Essex, and Beltsville) had less NO_2 than the model throughout the free troposphere, and Edgewood also exhibited an elevated NO_2 layer at 970 hPa not captured in the model.

Lamsal et al. (2014) also noted that there was significant day-to-day variability in the measured profiles that cannot be captured by a monthly average model; however, they do not quantify those differences. These day-to-day differences can be significant in a priori NO_2 profiles. Valin et al. (2013) showed that the concentration of NO_2 downwind of a city increases significantly with wind speed. When monthly average a priori profiles are used, this is not accounted for in the retrieval. The effect on the AMF is illustrated in Fig. 1c. Compared to the monthly average a priori profiles, daily profiles from a day with fast winds would contain greater near-surface NO_2 further from the city. UV/visible satellite observations of NO_2 are less sensitive to NO_2 at low altitudes, so this requires smaller AMFs at a greater distance from the city on days with fast winds to compensate through Eq. (1).

These day-to-day variations may be particularly important for methods such as Beirle et al. (2011), Valin et al. (2013), Lu et al. (2015), and Liu et al. (2016) that use observations sorted by wind speed to derive detailed information about NO_x chemistry and emissions from space-borne observations. This is a very valuable tool because of the wealth of data available from OMI (Levelt et al., 2006) and expected from upcoming instruments such as TROPOMI (Veefkind et al., 2012), TEMPO (Chance et al., 2013), Sentinel-4 (Ingmann et al., 2012), and GEMS (Bak et al., 2013; Choi and Ho, 2015). However, the act of sorting data by wind speed transforms errors in the profile shape resulting from day-to-day variability in wind speed from

Atmos. Chem. Phys. Discuss., doi:10.5194/acp-2016-536, 2016
Manuscript under review for journal Atmos. Chem. Phys.
Published: 12 July 2016

Atmospheric Chemistry and Physics Discussions

random to systematic. For example, Beirle et al. (2011), Valin et al. (2013), and Lu et al. (2015) derive an effective NO_x lifetime using data with fast wind speed, and Liu et al. (2016) does so by fitting a function with a component derived at slow wind speeds to data derived from days with fast wind speeds. On a day when the wind speed is faster than average, a priori NO_2 profiles taken from a monthly average model would have less near-surface NO_2 further from the city than is actually present for that day (i.e. Fig. 1c vs. 1a). The resulting incorrect AMFs would lead to an underestimation of the spatial extent of the plume, and could lead to an underestimate of the NO_x lifetime as a consequence.

In this paper we explore how day-to-day changes in the a priori NO_2 profiles will affect satellite retrievals of urban NO_2. In Fig. 1a, the monthly average NO_2 plume is shown as the grayscale gradient, to emphasize that it is static from day to day. Most of the plume follows the prevailing wind direction (here, to the right), but because days with different wind directions are averaged together, there is some influence of the plume upwind of the city. Figure 1b shows a case where the daily winds are similar to the monthly average. This leads to a similar NO_2 plume as in the monthly average, but because we are not averaging different wind directions, the upwind plume influence is removed (increasing the AMF, reflecting the reduction in near-surface NO_2) and conversely the downwind AMFs are slightly smaller, due to a slight increase in near-surface NO_2 from not averaging in days when the wind direction is different. Figure 1c shows a case where the daily winds are faster than the average. Here the AMFs within the city need to be larger, as near-surface NO_2 is being removed more efficiently and transported downwind, where the AMFs must therefore be smaller. Finally, Fig. 1d has the wind change direction from the monthly average. Left of the city must have smaller AMFs to account for the presence of the plume not seen in the monthly average, and the opposite change occurs to the right.

To do so, we combine the high spatial resolution a priori previously developed as part of the BErkeley High Resolution (BEHR) algorithm (Russell et al., 2011) with high temporal resolution to demonstrate the impact of day-to-day variations in the modeled NO_2 profiles on the calculated AMFs surrounding a major urban area such as Atlanta, GA. We show that this variability is largely due to changes in wind speed and direction. We first isolate the effects of day-to-day variations in boundary layer NO_2 alone (retaining a monthly average a priori profile in the free troposphere) on AMFs for the region surrounding Atlanta, then fully implement 91 days of retrieval to examine the effect on both day-to-day and monthly average NO_2 columns. Finally, we apply the EMG fitting method of Lu et al. (2015) to the new retrieval and show that the spatial and temporal resolution of the a priori profiles can significantly alter the derived emission rate and lifetime.

2 Methods

2.1 The Ozone Monitoring Instrument

The Ozone Monitoring Instrument (OMI), onboard the Aura satellite, is a polar-orbiting, nadir-viewing, UV-visible spectrometer with a swath width of 2600 km and a pixel size at nadir of 13×24 km. It observes backscattered solar radiation in the range of 270–500 nm with an average spectral resolution of 0.5 nm. (Levelt et al., 2006). It has a continuous data record since 1 Oct 2004, with theoretical global daily coverage. Since 25 June 2007, anomalous radiances have been observed in several of the pixel rows. These have been classified as the "row anomaly" and as of 5 July 2011 affect one-third of the pix-

Atmos. Chem. Phys. Discuss., doi:10.5194/acp-2016-536, 2016
Manuscript under review for journal Atmos. Chem. Phys.
Published: 12 July 2016

Atmospheric Chemistry and Physics Discussions

els (http://projects.knmi.nl/omi/research/product/rowanomaly-background.php), reducing coverage from global daily to global every two days. There are two publicly available global NO_2 products, the KNMI DOMINO product (Boersma et al., 2011) and the NASA Standard Product (Bucsela et al., 2013).

2.2 BEHR Retrieval

The BErkeley High Resolution (BEHR) retrieval is described in detail in Russell et al. (2011). Briefly, the BEHR retrieval uses the tropospheric SCD from the NASA OMNO2 retrieval (Bucsela et al., 2013) as a starting point. The radiance fitting, stratospheric subtration, and destriping is thus the same as the NASA OMNO2 retrieval. The tropospheric AMF is then recalculated similarly to the AMF formalism described in Palmer et al. (2001). Clear and cloudy AMFs are calculated as shown in Eq. (2). $w_s(p)$ represents scattering weights derived from the NASA OMNO2 look up table. $g(p)$ represents the mixing ratio NO_2 a priori profile taken from WRF-Chem, simulated at 12 km resolution in the published BEHR product. p_0 represents the surface pressure (clear sky AMF) or cloud pressure (cloudy AMF) of the satellite pixel, and p_{tp} the tropopause pressure. The integration is carried out using the scheme described in Ziemke et al. (2001) which allows integration of mixing ratio over pressure.

$$\mathrm{AMF} = \int_{p_0}^{p_{\mathrm{tp}}} w(p) S(p)\, dp \tag{2}$$

where

$$S(p) = \frac{1}{\int_{p_0}^{p_{\mathrm{tp}}} g(p)\, dp} g(p) \tag{3}$$

The scattering weights, $w(p)$, depend on the viewing geometry, surface albedo, and terrain pressure altitude. The BEHR algorithm uses the $0.05^\circ \times 0.05^\circ$ combined MODIS MCD43C3 black-sky albedo product and a surface pressure derived from the Global Land One-km Base Elevation project database (http://www.ngdc.noaa.gov/mgg/topo/globe.html; Hastings and Dunbar 1999) with a 7.4 km scale height as inputs to the clear sky scattering weights. Cloudy scattering weights treat the cloud pressure as the surface pressure and use an assumed cloud albedo of 0.8. The final AMF is computed as the cloud radiance fraction (f) weighted average of the clear and cloudy AMFs (Eq. 4).

$$\mathrm{AMF}_{\mathrm{total}} = f\mathrm{AMF}_{\mathrm{cloudy}} + (1-f)\mathrm{AMF}_{\mathrm{clear}} \tag{4}$$

The BEHR retrieval is available at http://behr.cchem.berkeley.edu/ for the continental US and southern Canada. Updates to the product since Russell et al. (2012) are detailed in the changelog at http://behr.cchem.berkeley.edu/Portals/2/Changelog.txt.

2.3 WRF-Chem

Modeled NO_2 a priori profiles are simulated using the WRF-Chem model (Grell et al., 2005). Meteorology is initialized with the North American Regional Reanalysis dataset. Anthropogenic emissions are taken from NEI11 and scaled to 88.9%

Atmos. Chem. Phys. Discuss., doi:10.5194/acp-2016-536, 2016
Manuscript under review for journal Atmos. Chem. Phys.
Published: 12 July 2016

Atmospheric Chemistry and Physics Discussions

to account for 2011–2013 NO_x reductions (EPA, 2016), and the MEGAN model is used to determine biogenic emissions. Boundary conditions for the domain are obtained from the MOZART chemical model. The RACM2 (Goliff et al., 2013) and MADE-SORGAM schemes are used to simulate gas-phase and aerosol chemistry respectively; the RACM2 scheme is customized to reflect recent advancements in understanding of alkyl nitrate chemistry (Browne et al., 2014; Zare, in prep).

The model is run from 27 May to 30 August, 2013. 27–31 May are treated as a spin up period, thus we use 1 June to 30 August as our study time period. Hourly NO_2 profiles from WRF-Chem are used as the a priori NO_2 profiles in the BEHR retrieval (Section 2.2). To produce monthly average profiles, each hourly profile is weighted according to Eq. (5), where l is the longitude of the profile and h is the hour (in UTC) that WRF calculated the profile for. The weights are clamped to the range $[0, 1]$. These are used as the weights in a temporal average over the month in question. This weighting scheme gives higher weights to profiles closest to the OMI overpass time around 1400 local standard time (to the nearest hour).

$$w_l = 1 - |14 - (l/15) - h| \tag{5}$$
$$w_l \in [0, 1]$$

A spatial resolution of 12 km is used as the high spatial resolution a priori. To determine the effect of coarser spatial resolution, the model is also run at 108 km resolution. At 12 km resolution, profiles are spatially matched to OMI pixels by averaging all profiles that fall within the pixel bounds. At 108 km resolution, the profile closest to the pixel is used. When using daily profiles, they are temporally matched by identifying those closest to the scan time defined in the Time field of the OMNO2 data product.

2.4 Implementation of daily profiles

Two retrievals are used to study the effects of incorporating daily a priori profiles in the BEHR algorithm. The first is what we term a "pseudo-retrieval" that is much simplified compared to a full operational NO_2 retrieval. This allows us to focus on the effects of daily a priori profiles, with fewer confounding variables. To create this retrieval, an 11×19 (across $\times$ along track) subset of pixels from OMI orbit 47335 centered on the pixel at $84.2513°$ W and $33.7720°$ N is used to provide the pixel corners, solar and viewing zenith and azimuth angles, terrain pressure, and terrain reflectivity. This swath places Atlanta near the nadir view of the OMI instrument (therefore providing pixels with good spatial resolution) while also remaining outside the row anomaly. This same subset of pixels is used for all days in the pseudo-retrieval. Cloud fractions are set to 0 for all pixels to consider clear-sky AMFs and simplify the pseudo-retrieval. AMFs are calculated for this subset of pixels with WRF-Chem NO_2 profiles from 1 June to 30 Aug 2013 in Eq. (2). This pseudo-retrieval will allow a simplified discussion of the effects of daily a priori profiles by:

1. Using a fixed set of OMI pixels. Because OMI pixels do not align day-to-day, using each day's true pixels makes a day-to-day comparison more difficult to see. In this pseudo-retrieval, that is alleviated.

Atmos. Chem. Phys. Discuss., doi:10.5194/acp-2016-536, 2016
Manuscript under review for journal Atmos. Chem. Phys.
Published: 12 July 2016

Atmospheric Chemistry and Physics Discussions

2. Using a fixed set of OMI pixels also keeps the scattering weights ($w(p)$ in Eq. 2) constant as the parameters that the scattering weights depend on (solar and viewing zenith angles, relative azimuth angles, terrain albedo, and terrain height) are fixed.

3. Setting cloud fractions to 0 ensures that the AMF for every pixel is calculated with the full a priori profile, rather than just the above cloud part. Day-to-day variations in cloud fraction also lead to large changes in AMF because a cloudy pixel will have a much greater AMF than a clear one, as it is more heavily weighted towards above cloud, higher altitude scattering weights which are greater than near-surface scattering weights.

Essentially, the pseudo-retrieval is a idealized experiment in which we hold all other variables except the a priori profile constant to compute the theoretical magnitude of the effect of using daily a priori profiles on the AMF. It will be used in Sect. 3.1 to demonstrate the effect of incorporating daily a priori profiles. The daily a priori profiles are also implemented in the full BEHR retrieval (no longer using a fixed set of pixels or forcing cloud fractions to 0) to determine the impact of including daily a priori profiles on the VCDs in a realistic case. To allow comparison between days with different OMI overpass tracks, all pixels are oversampled to a $0.05° \times 0.05°$ grid. When averaging over time, the contribution of each pixel is weighted by the inverse of its area.

2.5 Evaluation of EMG fits

Lu et al. (2015) and Valin et al. (2013) used NO_2 data from the NASA OMNO2 retrieval to study NO_x emissions and lifetime from space. To evaluate the impact of the a priori resolution on methods such as these, a similar procedure to fit an exponentially modified Gaussian function to NO_2 line densities is used. The surface wind direction and speed are calculated as the average of the first five layers of the 9 WRF 12 km grid cells closest to Atlanta for each day after WRF wind fields are transformed from grid-relative to earth-relative (http://www2.mmm.ucar.edu/wrf/users/FAQ_files/Miscellaneous.html) as:

$$U_{\text{earth}} = U_{\text{model}} \times \cos(\alpha) - V_{\text{model}} \times \sin(\alpha) \tag{6}$$

$$V_{\text{earth}} = V_{\text{model}} \times \cos(\alpha) + U_{\text{model}} \times \sin(\alpha) \tag{7}$$

where U and V are the longitudinal and latitudinal wind fields, and $\cos(\alpha)$ and $\sin(\alpha)$ are outputs from WRF as the variables COSALPHA and SINALPHA.

As in Valin et al. (2013), the satellite pixels are rotated so that wind direction (and therefore NO_2 plumes) for each day lie along the x-axis. Pixels affected by the row anomaly or with a cloud fraction $> 20\%$ are removed. Pixels within $1°$ upwind and $2°$ downwind are gridded to $0.05° \times 0.05°$ and integrated across $1°$ perpendicular to the x-axis. This produces line densities, which are a one-dimensional representation of the NO_2 concentration at various distances downwind of the city. Three a priori sets are used to create the retrievals used in this section: coarse (108 km) monthly average, fine (12 km) monthly average, and fine (12 km) daily profiles.

Atmos. Chem. Phys. Discuss., doi:10.5194/acp-2016-536, 2016
Manuscript under review for journal Atmos. Chem. Phys.
Published: 12 July 2016

Atmospheric Chemistry and Physics Discussions

We use the form of the EMG function described in Lu et al. (2015) to fit the calculated NO_2 line densities, after expanding the definition of the cumulative distribution function:

$$F(x|a,x_0,\mu_x,\sigma_x,B) = \frac{a}{2x_0}\exp\left(\frac{\mu_x}{x_0}+\frac{\sigma_x^2}{2x_0^2}-\frac{x}{x_0}\right)\mathrm{erfc}\left(-\frac{1}{\sqrt{2}}\left[\frac{x-\mu_x}{\sigma_x}-\frac{\sigma_x}{x_0}\right]\right)+B \quad (8)$$

and find the values of a, x_0, μ_x, σ_x, and B that minimize the sum of squared residuals:

$$Resid(a,x_0,\mu_x,\sigma_x,B) = \sum_x \left(F(x|a,x_0,\mu_x,\sigma_x,B) - \mathrm{NO_2}(x)\right)^2 \quad (9)$$

The Matlab function fmincon is used to minimize Eq. (9), finding the values of a, x_0, μ_x, σ_x, and B that best fit the line densities. The values of a, x_0, μ_x, σ_x, and B have physical significance (enumerated in Table 1) and so their optimum values yield information about the NO_x emission and chemistry occurring within the plume. In practice, several additional refinements to the algorithm are necessary to properly fit the line densities:

- The constraints listed in Table 1 must be imposed to ensure physically realistic values of a, x_0, μ_x, σ_x, and B are obtained.

- Any not-a-number (NaN) values in the EMG function (Eq. 8) are replaced with infinity, thus making the fitting function (Eq. 9) report that the current values of a, x_0, μ_x, σ_x, and B are unacceptable. NaNs occur in the EMG function when the exponential goes to infinity and the error function to zero, typically when the fitting parameters are unrealistically large or small and the fit is incorrectly a flat line. By doing this replacement and using the Matlab function nansum (which ignores NaNs during the summation but will return 0 if all values are NaN) to do the summation in Eq. (9), we allow NaNs to occur in the line densities (representing missing data, which is thus ignored) but not the fit.

- fmincon requires an initial value for a, x_0, μ_x, σ_x, and B. For the first minimization, best-guess values for these are computed as specified in Table 1 (see supplement for rationale for each). However, fmincon uses an interior-point minimization algorithm by default. Such algorithms use a line search strategy which minimizes a function by following the derivative at the current point "downhill" (Robere, 2012; Wright, 2005). If the algorithm begins in a region from which the downhill path leads to a local, rather than global, minimum, the global minimum may never be found by this algorithm. This can be alleviated by carrying out multiple minimizations, starting from a different point each time, and choosing the result with the smallest residual. The randomization draws from the range of values defined by the upper and lower limits for each parameter with a uniform probability distribution. For a and x_0, upper bounds of 5×10^6 mol and 1000 km, respectively, are used during the randomization process, as a finite upper bound is necessary for the randomization algorithm. This randomization and reoptimization was carried out nine times per fit. Additional randomization of the initial point does not improve the fit. Each time the optimum value of the fitting function is compared to the previous minimum; if it is less, the new fit is accepted.

Atmos. Chem. Phys. Discuss., doi:10.5194/acp-2016-536, 2016
Manuscript under review for journal Atmos. Chem. Phys.
Published: 12 July 2016

Atmospheric Chemistry and Physics Discussions

For each parameter, uncertainty from the fitting process itself is computed as the 95% confidence interval calculated using the standard deviation obtained from the fitting process. This is combined in quadrature with 10% uncertainty due to across wind integration distance, 10% uncertainty due to the choice of wind fields, and $25\%/\sqrt{n}$ uncertainty from the VCDs, similar to Beirle et al. (2011) and Lu et al. (2015). A full description of this calculation is provided in the supplement.

3 Results

3.1 Daily variations

Fig. 2 shows the average wind and modeled NO_2 columns for June 2013, and the AMF values for the psuedo-retrieval around Atlanta, GA. Atlanta was chosen as the focus of this study because it represents a strong NO_x source relatively isolated from other equally large sources. This ensures that changes to the a priori profiles on a daily basis can be attributed to a local cause. The prevailing wind pattern advects NO_2 to the northeast of Atlanta (the location of Atlanta is marked by the star), as can be seen in the wind field shown in Fig. 2b and the WRF-Chem NO_2 columns in Fig. 2c. The average surface wind speed over Atlanta for June is 3.9 m/s. This distribution of NO_2 leads directly to the lower AMFs seen to the northeast of Atlanta in Fig. 2d through Eq. (2).

To illustrate the effect of incorporating daily a priori profiles into the retrieval, we consider two days: 18 and 22 June 2013. These provide an illustration of the effect of changes in both wind speed and direction. Figure 3a–c shows the result from implementing the daily profiles for 22 June. On this day, the winds over Atlanta blow out of Atlanta to the northwest, with a speed at the surface of 3.6 m/s. This is similar to the monthly average speed (3.9 m s^{-1}) but are rotated 90° counterclockwise compared with the monthly average. The change in direction results in much greater near-surface NO_2 to the northwest compared to the monthly average (Fig. 3b) as the wind direction advects NO_2 into an area with low NO_2 in the monthly average.

Figure 3c shows that the greater near-surface NO_2 to the northwest results in lower AMFs than average (red), while the opposite is true to the east (blue). The greater near-surface NO_2 in profiles to the northwest weights $S(p)$ in Eq. (2) more heavily towards lower altitudes, where $w(p)$ is less, thus decreasing the overall AMF by ∼15%. The increase in AMFs to the east reflects the inflow of cleaner air from the shift in winds. This reduces near-surface NO_2 and increases the weight of higher altitudes of $S(p)$, increasing the AMFs by 26–37% (the colorbar saturates at $\pm 25\%$ to make the decrease to the northwest easier to see).

Wind speed also plays an important role in determining the a priori profile shape through transport and chemistry. Fig. 3d–f shows results from 18 June, where the wind speed over Atlanta averaged 6.8 m/s. This results in faster advection away from emission sources, with 10–15% increases in modeled NO_2 columns to the west as the plume is driven east more strongly. The greatest decreases in AMF (and thus increases in VCD) are as much as -11% and occur between 84° and 83° W where the increased wind speed has advected the NO_2 plume farther than the average. There is also a 2–10% increase along the east edge of Atlanta, resulting from the shift of the plume center east.

When the change in AMF from using the hybrid daily a priori profiles is averaged over the full time period studied (1 June–30 Aug), the percent change in AMF is on average +3.6% throughout the domain with a maximum of +9.8%. All pixels show a

Atmos. Chem. Phys. Discuss., doi:10.5194/acp-2016-536, 2016
Manuscript under review for journal Atmos. Chem. Phys.
Published: 12 July 2016

Atmospheric Chemistry and Physics Discussions

positive change. 77% of the daily profiles have less NO_2 than the corresponding monthly average profile, as most pixels will be upwind from the city on any given day and will see a decrease in NO_2 when upwind and downwind days are no longer averaged together. This reduces the denominator in Eq. (3) and increases the contribution of upper tropospheric scattering weights to the AMF. Scattering weights increase with altitude; therefore, this results in a systematic increase of the AMF throughout the domain for the pseudo-retrieval.

We also consider the relative importance of day-to-day changes in the boundary layer of the a priori profiles versus day-to-day changes in the free troposphere of the a priori profiles by running the pseudo-retrieval with a set of hybrid daily profiles that only include day-to-day variability below 750 hPa and use a monthly average profile above that. The changes in AMFs using these hybrid profiles versus monthly average profiles are very similar to those observed when using the full daily profiles. In general, the hybrid profiles has a slightly greater average increase in AMFs ($+4.2\%$ vs. $+3.6\%$) and slightly less extreme changes, but the overall distribution of changes in AMFs is very similar. From this, we can conclude that changes in the boundary layer of the a priori profiles are the dominant reason for changes to the AMFs. However, the WRF-Chem simulations used to produce the a priori profiles did not include lightning NO_x, so this should be considered a lower bound for the effect of day-to-day changes in the free troposphere. The detailed comparison is described in the supplement.

3.2 Effects on retrieved VCDs in full retrieval

To determine the effect the inclusion of daily a priori profiles has on the final retrieved VCDs, the daily profiles were implemented in the full BEHR retrieval. Effects on individual days and multi-month average VCDs are presented here. The cities of Birmingham, AL and Montgomery, AL are included to demonstrate that this effect is significant for cities of various sizes. Atlanta, GA is the largest with approximately 5.7 million people, followed by Birmingham, AL with 1.1 million, and Montgomery, AL with 374,000 (United States Census Bureau). For simplicity, we will consider changes significant if they are greater than the global mean uncertainty of 1×10^{15} molec. cm^{-2} in tropospheric vertical column densities computed by Bucsela et al. (2013) for the NASA OMNO2 OMI NO_2 product version 2.1.

Table 2 describes how frequently significant ($> 1 \times 10^{15}$ molec. cm^{-2}) changes in the retrieved VCD occur for pixels within 50 km of Atlanta, Birmingham, and Montgomery. We consider the fraction of days with at least one pixel exhibiting a significant change in VCD (rather than the fraction of pixels) because the main NO_2 plume may only fall within a small number of pixels. Approximately one-third to two-thirds of days will exhibit changes in the VCDs greater than 1×10^{15} molec. cm^{-2}. This indicates that when considering individual daily measurements, a considerable fraction of days with any valid pixels would have biases in the retrieved VCDs above the global mean uncertainty due to the temporal resolution of the a priori NO_2 profiles.

Table 2 also indicates that Birmingham and its surrounding area exhibits the largest and most frequent changes when using a daily a priori profile. Figure 4a shows the NO emissions throughout this domain. Birmingham has the second largest NO_x emission rate, after Atlanta, while Montgomery has the smallest of the three cities considered. We note that the largest changes are not associated with the city with the greatest NO_x emissions. Both Atlanta and Birmingham fall entirely within the NO_x suppressed regime in the model, so the larger changes in Birmingham are not because NO_x chemistry transitions between the

Atmos. Chem. Phys. Discuss., doi:10.5194/acp-2016-536, 2016
Manuscript under review for journal Atmos. Chem. Phys.
Published: 12 July 2016

Atmospheric Chemistry and Physics Discussions

NO_x suppressed and NO_x limited regimes. Instead, the magnitude of these changes is due to Birmingham's intermediate size, where significant NO_2 is present, but emission occurs over a small enough area that changes in wind direction can significantly affect NO_2 concentration at a short distance from the source. Montgomery has the least frequent significant changes because it has the smallest VCDs, so a change to the AMF needs to be rather large to produce a significant change in the VCD, since the AMF is a multiplicative factor.

Implementing the daily profiles also changes the average VCDs, in addition to the day-to-day changes in VCDs discussed above. Figure 4b shows the changes in VCDs averaged over the period studied. The main decrease around Atlanta is to the northeast, along the direction that the monthly average model results placed the NO_2 plume. A systematic decrease of 5–10% to the northeast of Atlanta is observed; this is the plume direction in the monthly average profiles. The absolute change is small (4×10^{14} molec. cm^{-2}) but this is above the uncertainty, as the nominal uncertainty of 1×10^{15} molec. cm^{-2} can be reduced by $\sqrt{40}$ for the number of observations (not impacted by clouds or the row anomaly), to $\sim 1.6 \times 10^{14}$ molec. cm^{-2}. The greatest changes are observed around the smaller cities of Birmingham (down to -13.8%) and Montgomery (down to -14.8%). This appears to be due primarily because the areas of emissions are smaller which makes shifts in wind direction have a greater average effect on the plume shape.

Unlike the pseudo-retrieval, where we only allowed the a priori profiles to vary day-to-day and clouds were set to zero, there is a some spatial structure to these average changes. This is primarily a statistical phenomenon. We use only pixels with cloud fraction $< 20\%$, which reduces the number of pixels in the average. Within this subset, the wind blows to the southeast out of Atlanta more frequently than other directions; so the increases due to properly accounting for the presence of surface NO_2 average with the more typical decreases to give a small average change. The other directions exhibit the expected average decrease in VCDs due to the average increase in AMFs discussed in section 3.1. We expect that over longer periods of time all directions would see a 2–6% decrease in the average VCDs.

4 Discussion

Recently several authors have used wind-sorted satellite NO_2 observations to probe NO_x chemistry and emissions from space (Beirle et al., 2011; Valin et al., 2013; de Foy et al., 2014; Lu et al., 2015; Liu et al., 2016). We apply the EMG fitting method of Lu et al. (2015) to NO_2 line densities derived from NO_2 columns retrieved using the daily and monthly average a priori profiles, as well as a monthly average profile simulated at 108 km resolution for both Atlanta and Birmingham. To match the method of Lu et al. (2015) as closely as possible, we use 3 m s^{-1} as the division between slow and fast winds.

We acknowledge that a 91 day averaging period is significantly shorter than those used in Beirle et al. (2011), Valin et al. (2013), or Lu et al. (2015) (5 years, summer half-year for 7 years, and summer half-year for 3 year periods, respectively). However, since the goal of this section is to compare the results obtained using three different sets of a priori profiles with all other variables equal, we believe that 91 days is sufficient for this purpose.

Additionally, we do not include days around Atlanta in which the wind blows towards the southeast (specifically 0° to -112.5°, 0° is defined as east, negative values are clockwise from east). Significant suburban NO_2 columns near 83.5° W, 33°

Atmos. Chem. Phys. Discuss., doi:10.5194/acp-2016-536, 2016
Manuscript under review for journal Atmos. Chem. Phys.
Published: 12 July 2016

Atmospheric Chemistry and Physics Discussions

N add a secondary maximum to the line densities which can erroneously lengthen the decay time of the fit. All wind directions are used for Birmingham.

Accounting for the spatial and temporal variability of NO_2 in the a priori profiles leads to several notable changes in the line densities and the resulting EMG fits. Figure 5 shows the line densities and the corresponding EMG fits around Atlanta for the average over the 91 day study period. Table 3 enumerates the values obtained for the fitting parameters in Eq. (8) for the fits of the Atlanta NO_2 plume in Fig. 5 and fits for the Birmingham NO_2 plume (not shown).

The spatial scale of the a priori makes the greatest difference to the maximum value of the line density, causing a significant increase in a when the spatial resolution of the a priori profiles increases from 108 km to 12 km. This reflects the impact of the blurring of urban and rural profiles described in Russell et al. (2011).

Both the spatial and temporal resolution impact the determination of x_0, the distance traveled in one lifetime. This parameter is determined at fast wind speeds (Lu et al., 2015; Valin et al., 2013), so we consider only the results for wind speed ≥ 3.0 m s^{-1}. For Atlanta, using a daily a priori results in an x_0 value 30% greater than that obtained using a monthly average profile at the same spatial resolution (12 km). The same comparison for Birmingham, AL shows a 66% increase in x_0 between the monthly and daily 12 km a priori.

μ_x represents the apparent center of the NO_2 plume relative to the geographic center of the city. This moves downwind (positive) when changing from the monthly average 12 km or 108 km a priori to the daily 12 km a priori. This reflects the ability of the daily a priori to capture how the wind distorts the plume shape.

σ_x is the Gaussian smoothing length scale, representing the width of the upwind Gaussian plume. There is a slight decrease when going from a monthly average to daily profiles, which reflects the general increase in upwind AMFs (i.e. compare Fig. 1a and 1b), but because this is outside of the main NO_2 plume, the effect is small.

Finally, B is the background line density. Ideally, it is derived sufficiently far from any NO_x sources that spatial and temporal variability should be minimal. Indeed, in three of the four cases any change in derived background is less than the uncertainty. When considering slow winds around Birmingham there is a $\sim 25\%$ increase when improving the spatial resolution of the a priori profiles. This is likely attributable to the general increase in urban signal discussed several times so far pulling the edges of the line density upward. However, a greater selection of cities is necessary to demonstrate this more conclusively.

Ultimately, the goal of this method is to extract information about chemically relevant quantities such as emission rate and lifetime. Since de Foy et al. (2014) showed that choice of wind speed bins affects the values obtained, we also consider if the effect of implementing the daily a priori profile changes if the observations are binned by different wind speed criteria. Table 4 compares the values of the NO_x emission rate, E, and effective lifetime, τ_{eff}, derived from different wind speed bins for Atlanta and Birmingham. Restricting the analysis to days with wind speed greater than 5 m s^{-1} results in too few days for a meaningful analysis around Atlanta (due to the need to remove days with winds to the southeast), so results for Atlanta are restricted to ≥ 3 m s^{-1} and ≥ 4 m s^{-1} only.

Atmos. Chem. Phys. Discuss., doi:10.5194/acp-2016-536, 2016
Manuscript under review for journal Atmos. Chem. Phys.
Published: 12 July 2016

Atmospheric Chemistry and Physics Discussions

τ_{eff} and E are each computed from several of the EMG fitting parameters. τ_{eff} depends on x_0 and w through Eq. (10):

$$\tau_{\text{eff}} = \frac{x_0}{w} \tag{10}$$

E depends on a, x_0, and w (the mean wind speed) through Eq. (11):

$$E = 1.32 \times \frac{a \times w}{x_0} = 1.32 \times \frac{a}{\tau_{\text{eff}}} \tag{11}$$

where the factor of 1.32 accounts for the NO_x:NO_2 ratio throughout the tropospheric column (Beirle et al., 2011).

Both Valin et al. (2013) and de Foy et al. (2014) show that lifetime should decrease at faster wind speeds. We see this trend for Birmingham but not Atlanta. de Foy et al. (2014) also saw that, for a chemical lifetime of 1 h, greater derived emissions were found at faster wind speeds. This is also better seen in our results for Birmingham than Atlanta. Previous measurements of NO_x lifetime in urban plumes which average 3.8 h and range from 2-6 h (Beirle et al., 2011; Ialongo et al., 2014; Nunnermacker et al., 1998; Spicer, 1982), and using the EMG method, Lu et al. (2015) saw effective lifetimes between 1.2 and 6.8 h. The lifetimes we calculate are at the low end of the previously observed ranges. However, this is similar to the instantaneous lifetime of 1.2 ± 0.5 h and 0.8 ± 0.4 h calculated from the WRF-Chem model for days in June 2013 with wind speed ≥ 3 m s^{-1} and grid cells within 50 km of Atlanta and Birmingham, respectively (see the supplement for the calculation details).

We use t-tests at the 95% confidence level (Harris, 2010) to determine if differences in emissions and lifetimes are significantly different among the results derived from using the three different a priori profile sets for a given city and wind speed bin (i.e. we compare the three values of emissions derived using different a priori profiles for Atlanta and wind speeds ≥ 3 m s^{-1}). For emissions, the choice of a priori leads to statistically different emissions for all five cases. For the derived lifetimes, in all cases the monthly 108 km and daily 12 km a priori are statistically indistinguishable, but the monthly 12 km a priori is statistically different.

We note that there is a systematic difference in the lifetimes derived using the daily and monthly 12 km a priori profiles. In all cases, the lifetime derived using the daily profiles is 30–50% longer. When using monthly average a priori profiles, profiles resulting from different wind directions are averaged together. The AMFs calculated from these profiles thus reflect the the average distance from the city the plume reaches in a given direction, e.g. east of the city, with smaller AMFs near the city and greater AMFs more distant (Fig. 1). In this hypothetical example, when the wind blows to the east, the spatial extent of the plume is underestimated because the average AMFs towards the end of the plume will be too large, so the VCDs will be too small by Eq. (1). On days when the wind does not blow east, the reverse is true: the plume extent is overestimated because the AMFs nearer to the city are too small (Fig. 1d). If one considers a simple average change in the VCDs, these two errors will partially cancel and we will see the average change from Sect. 3.2. However, in the EMG fitting approach, these errors do not cancel at all because the EMG method both rotates the NO_2 plumes so that the wind directions align before calculating the line densities and systematically selects fast winds to determine τ_{eff}, so we are always dealing with the first case and the plume extent is always underestimated. In the EMG fit, this manifests as a too short lifetime. Therefore, when using a retrieval with a

Atmos. Chem. Phys. Discuss., doi:10.5194/acp-2016-536, 2016
Manuscript under review for journal Atmos. Chem. Phys.
Published: 12 July 2016

Atmospheric Chemistry and Physics Discussions

priori profile at fine spatial resolution, daily temporal resolution of the a priori profiles is necessary to prevent underestimating the lifetime.

We also compare the derived emissions rates to the emissions in a 12 km WRF-Chem model driven by the NEI 11 emission inventory with NO_x emissions scaled to 88.9% of the 2011 values to account for the decrease between 2011 and 2013 (EPA, 2016). WRF-Chem emissions are calculated as the sum of all grid cells within a 50 km radius of the city. 50 km was chosen as the line densities were integrated for ~ 50 km to either side perpendicular to the wind direction. The coarse monthly a priori are 43–62% lower than the NEI-driven emissions, while emissions derived using daily 12 km a priori are within 5–24%. Recent work (e.g. Travis et al. 2016 and references within) suggests that the NEI inventory is overestimated by $\sim 50\%$ using both satellite and in situ observations. Therefore, we cannot say which a priori profiles provide the best measurement of emissions by comparing to NEI. It is likely that emissions derived using the monthly 12 km a priori profiles are an overestimate, possibly because the systematically low lifetimes discussed above increase E through Eq. (11). Emissions derived using daily 12 km and monthly 108 km a priori profile agree with the current and 50% reduced NEI emissions, respectively. From this, it is clear the choice of a priori profiles has a substantial impact on emissions derived from satellite observations, and that both spatial and temporal resolution of the a priori profiles contribute to that difference, and further work is needed to fully evaluate this impact in light of work such as Travis et al. (2016).

In summary, the two most important parameters (a and x_0) and values derived from them (E, τ_{eff}) are significantly affected by the spatial and temporal resolution of the a priori. a and is most affected by increasing the spatial resolution of the a priori, while using daily profiles corrects a systematic bias in x_0 when the profiles are simulated at high spatial resolution. E is affected by both the spatial and temporal resolution of the a priori profiles, increasing by $\sim 100\%$ between the retrievals using coarse monthly and fine daily a priori profiles. Therefore the use of daily a priori NO_2 profiles at high spatial resolution significantly alters the results obtained from fitting wind aligned retrieved NO_2 columns with an analytical function. This will be most important when considering absolute measurements rather than trends, as the systematic biases should cancel out in a trend analysis.

5 Conclusions

We have demonstrated that incorporating daily NO_2 a priori profiles simulated at sufficiently fine spatial scales to capture the spatial variation of an NO_2 plume leads to significant changes in the final VCDs when compared to monthly average profiles at the same spatial resolution. Changes to VCDs on a single day are up to 40% (relative) and 3×10^{15} molec. cm^{-2} (absolute). This is attributable to changes in the direction of the NO_2 plume. Up to 59% of days with valid observations exhibit changes in VCDs $> 1 \times 10^{15}$ molec. cm^{-2}. Additionally, the inclusion of daily profiles affects a systematic change in time-averaged VCDs around Atlanta, GA. Pixels downwind in the average exhibited VCD decreases up to 10% (0.4×10^{15} molec. cm^{-2}). Day-to-day variations in the free troposphere have a smaller impact on the value of the AMF, and average out to no net change over the period studied. These results were obtained using WRF-Chem without lightning NO_x emissions; it is likely that the

Atmos. Chem. Phys. Discuss., doi:10.5194/acp-2016-536, 2016
Manuscript under review for journal Atmos. Chem. Phys.
Published: 12 July 2016

Atmospheric Chemistry and Physics Discussions

inclusion of lightning NO_x would increase the magnitude of positive changes to the AMF due to the presence of NO_2 at altitude to which OMI is highly sensitive.

When the methods of Lu et al. (2015) are applied to these prototype retrievals, significant changes in derived NO_x emissions are found, increasing by as much as 100% for Atlanta. Using high spatial resolution, monthly average a priori profiles results in the highest derived emissions rates, followed by high spatial resolution, daily a priori, with spatially coarse a priori leading to the lowest derived emissions. Further work is needed to understand the impact of this change on top down constraints of NO_x emissions, given the recent work showing that bottom up estimates are high by $\sim 50\%$. Lifetimes derived from satellite observations using a spatially fine but monthly averaged a priori are systematically biased low due to the spatial pattern of AMF imposed by such a priori; the use of daily profiles at fine spatial resolution corrects this systematic bias.

Having shown that the use of daily a priori NO_2 profiles in the retrieval algorithm significantly alters emissions and lifetimes derived from this retrieval, we plan to implement such profiles for several years at the beginning and current end of the OMI data record to investigate how NO_x lifetimes have changed in urban plumes over the past decade. Such work can provide a greater understanding of the most effective means of improving air quality in years to come, as it will allow us to determine whether reductions in NO_x or VOC emissions will provide the most benefit in ozone reduction.

Acknowledgements. The authors gratefully acknowledge support from the NASA ESS Fellowship NNX14AK89H, NASA grants NNX15AE37G and NNX14AH04G, and the TEMPO project grant SV3-83019. The MODIS Aqua L2 Clouds 5-Min Swath 1km and 5 km (MYD06_L2) and MODIS Terra+Aqua Albedo 16-Day L3 Global 0.05Deg CMG V005 were acquired from the Level-1 and Atmospheric Archive and Distribution System (LAADS) Distributed Active Archive Center (DAAC), located in the Goddard Space Flight Center in Greenbelt, Maryland (https://ladsweb.nascom.nasa.gov/). This research used the Savio computational cluster resource provided by the Berkeley Research Computing program at the University of California, Berkeley (supported by the UC Berkeley Chancellor, Vice Chancellor of Research, and Office of the CIO).

Atmos. Chem. Phys. Discuss., doi:10.5194/acp-2016-536, 2016
Manuscript under review for journal Atmos. Chem. Phys.
Published: 12 July 2016

Atmospheric Chemistry and Physics Discussions

References

Bak, J., Kim, J. H., Liu, X., Chance, K., and Kim, J.: Evaluation of ozone profile and tropospheric ozone retrievals from GEMS and OMI spectra, Atmos. Meas. Tech., 6, 239–249, doi:10.5194/amt-6-239-2013, 2013.

Beirle, S., Huntrieser, H., and Wagner, T.: Direct satellite observations of lightning-produced NO_x, Atmos. Chem. Phys., 10, 10 965–10 986, doi:10.5194/acp-10-10965-2010, 2010.

Beirle, S., Boersma, K., Platt, U., Lawrence, M., and Wagner, T.: "Megacity Emissions and Lifetimes of Nitrogen Oxides Probed from Space", Science, 333, 1737–1739, 2011.

Boersma, K., Eskes, H., Dirksen, R., van der A, R., Veefkind, J., Stammes, P., Huijnen, V., Kleipool, Q., Sneep, M., Claas, J., Leitão, J., Richter, A., Zhou, Y., and Brunner, D.: "An improved tropospheric NO_2 column retrieval algorithm for the Ozone Monitoring Instrument, Atmos. Meas. Tech., 4, 1905–1928, doi:10.5194/amt-4-1905-2011, 2011.

Browne, E. C., Wooldridge, P. J., Min, K.-E., and Cohen, R. C.: On the role of monoterpene chemistry in the remote continental boundary layer, Atmospheric Chemistry and Physics, 14, 1225–1238, doi:10.5194/acp-14-1225-2014, 2014.

Bucsela, E., Krotkov, N., Celarier, E., Lamsal, L., Swartz, W., Bhartia, P., Boersma, K., Veefkind, J., Gleason, J., and Pickering, K.: "A new tropospheric and stratospheric NO_2 retrieval algorithm for nadir-viewing satellite instruments: applications to OMI, Atmos. Meas. Tech., 6, 2607–2626, doi:10.5194/amt-6-2607-2013, 2013.

Castellanos, P., Boersma, K. F., and van der Werf, G. R.: Satellite observations indicate substantial spatiotemporal variability in biomass burning NO_x emission factors for South America, Atmos. Chem. Phys., 14, 3929–3943, doi:10.5194/acp-14-3929-2014, 2014.

Chance, K., Liu, X., Suleiman, R. M., Flittner, D. E., Al-Saadi, J., and Janz, S. J.: Tropospheric emissions: monitoring of pollution (TEMPO), doi:10.1117/12.2024479, 2013.

Choi, Y.-S. and Ho, C.-H.: Earth and environmental remote sensing community in South Korea: A review, Remote Sensing Applications: Society and Environment, 2, 66–76, doi:http://dx.doi.org/10.1016/j.rsase.2015.11.003, 2015.

Cohan, D. S., Hu, Y., and Russell, A. G.: Dependence of ozone sensitivity analysis on grid resolution, Atmos. Environ., 40, 126–135, doi:http://dx.doi.org/10.1016/j.atmosenv.2005.09.031, 2006.

de Foy, B., Wilkins, J., Lu, Z., Streets, D., and Duncan, B.: Model evaluation of methods for estimating surface emissions and chemical lifetimes from satellite data, Atmos. Environ., 98, 66–77, doi:10.1016/j.atmosenv.2014.08.051, 2014.

Ding, J., van der A, R. J., Mijling, B., Levelt, P. F., and Hao, N.: NO_x emission estimates during the 2014 Youth Olympic Games in Nanjing, Atmospheric Chemistry and Physics, 15, 9399–9412, doi:10.5194/acp-15-9399-2015, 2015.

EPA: Air Pollutant Emissions Trends Data, https://www.epa.gov/air-emissions-inventories/air-pollutant-emissions-trends-data, 2016.

Goliff, W. S., Stockwell, W. R., and Lawson, C. V.: The regional atmospheric chemistry mechanism, version 2, Atmos. Environ., 68, 174 – 185, doi:http://dx.doi.org/10.1016/j.atmosenv.2012.11.038, 2013.

Grell, G. A., Peckham, S. E., Schmitz, R., McKeen, S. A., Frost, G., Skamarock, W. C., and Eder, B.: Fully coupled "online" chemistry within the {WRF} model, Atmospheric Environment, 39, 6957 – 6975, doi:http://dx.doi.org/10.1016/j.atmosenv.2005.04.027, 2005.

Gu, D., Wang, Y., Smeltzer, C., and Liu, Z.: Reduction in NOx Emission Trends over China: Regional and Seasonal Variations, Environ. Sci. Technol., 47, 12 912–12 919, doi:10.1021/es401727e, 2013.

Harris, D.: Comparison of Means with Student's t, chap. 4-3, pp. 76–78, W.H. Freeman, 8th edn., 2010.

Hastings, D. and Dunbar, P.: Global Land One-kilometer Base Elevation (GLOBE) Digital Elevation Model, Documentation, Volume 1.0. National Oceanic and Atmospheric Administration, National Geophysical Data Center, 325 Broadway, Boulder, Colorado 80303, U.S.A., 1999.

Heckel, A., Kim, S.-W., Frost, G. J., Richter, A., Trainer, M., and Burrows, J. P.: Influence of low spatial resolution a priori data on tropospheric NO_2 satellite retrievals, Atmos. Meas. Tech., 4, 1805–1820, doi:10.5194/amt-4-1805-2011, 2011.

Huang, M., Bowman, K. W., Carmichael, G. R., Chai, T., Pierce, R. B., Worden, J. R., Luo, M., Pollack, I. B., Ryerson, T. B., Nowak, J. B., Neuman, J. A., Roberts, J. M., Atlas, E. L., and Blake, D. R.: Changes in nitrogen oxides emissions in California during 2005–2010 indicated from top-down and bottom-up emission estimates, J. Geophys. Res. Atmos., 119, 12,928–12,952, doi:10.1002/2014JD022268, 2014.

Ialongo, I., Hakkarainen, J., Hyttinen, N., Jalkanen, J.-P., Johansson, L., Boersma, K. F., Krotkov, N., and Tamminen, J.: Characterization of OMI tropospheric NO_2 over the Baltic Sea region, Atmos. Chem. Phys., 14, 7795–7805, doi:10.5194/acp-14-7795-2014, 2014.

Ingmann, P., Veihelmann, B., Langen, J., Lamarre, D., Stark, H., and Courrèges-Lacoste, G. B.: Requirements for the {GMES} Atmosphere Service and ESA's implementation concept: Sentinels-4/-5 and -5p, Remote Sens. of Environ., 120, 58–69, doi:http://dx.doi.org/10.1016/j.rse.2012.01.023, 2012.

Kim, S.-W., Heckel, A., Frost, G. J., Richter, A., Gleason, J., Burrows, J. P., McKeen, S., Hsie, E.-Y., Granier, C., and Trainer, M.: NO2 columns in the western United States observed from space and simulated by a regional chemistry model and their implications for NOx emissions, J. Geophys. Res. Atmos., 114, doi:10.1029/2008JD011343, 2009.

Krotkov, N. and Veefkind, P.: OMI/Aura Nitrogen Dioxide (NO2) Total and Tropospheric Column 1-orbit L2 Swath 13x24 km V003, version 003, Greenbelt, MD, USA, Goddard Earth Sciences Data and Information Services Center (GES DISC), accessed 19 May 2014, doi:10.5067/Aura/OMI/DATA2017.

Kuhlmann, G., Lam, Y. F., Cheung, H. M., Hartl, A., Fung, J. C. H., Chan, P. W., and Wenig, M. O.: Development of a custom $OMINO_2$ data product for evaluating biases in a regional chemistry transport model, Atmos. Chem. Phys., 15, 5627–5644, doi:10.5194/acp-15-5627-2015, 2015.

Lamsal, L. N., Krotkov, N. A., Celarier, E. A., Swartz, W. H., Pickering, K. E., Bucsela, E. J., Gleason, J. F., Martin, R. V., Philip, S., Irie, H., Cede, A., Herman, J., Weinheimer, A., Szykman, J. J., and Knepp, T. N.: Evaluation of OMI operational standard NO_2 column retrievals using in situ and surface-based NO_2 observations, Atmospheric Chemistry and Physics, 14, 11 587–11 609, doi:10.5194/acp-14-11587-2014, 2014.

Lamsal, L. N., Duncan, B. N., Yoshida, Y., Krotkov, N. A., Pickering, K. E., Streets, D. G., and Lu, Z.: U.S. NO_2 trends (2005–2013): EPA Air Quality System (AQS) data versus improved observations from the Ozone Monitoring Instrument (OMI), Atmos. Environ., 110, 130–143, doi:http://dx.doi.org/10.1016/j.atmosenv.2015.03.055, 2015.

Levelt, P., van der Oord, G., Dobber, M., Mälkki, A., Visser, H., de Vries, J., Stammes, P., Lundell, J., and Saari, H.: The Ozone Monitoring Instrument, IEEE Trans. Geosci. Remote Sense., 44, 1093–1101, doi:10.1109/TGRS.2006.872333, 2006.

Lin, J.-T., McElroy, M. B., and Boersma, K. F.: Constraint of anthropogenic NO_x emissions in China from different sectors: a new methodology using multiple satellite retrievals, Atmos. Chem. and Phys., 10, 63–78, doi:10.5194/acp-10-63-2010, 2010.

Lin, J.-T., Liu, M.-Y., Xin, J.-Y., Boersma, K. F., Spurr, R., Martin, R., and Zhang, Q.: Influence of aerosols and surface reflectance on satellite NO_2 retrieval: seasonal and spatial characteristics and implications for NO_x emission constraints, Atmos. Chem. Phys., 15, 11 217–11 241, doi:10.5194/acp-15-11217-2015, 2015.

Liu, F., Beirle, S., Zhang, Q., Dörner, S., He, K., and Wagner, T.: NOx lifetimes and emissions of cities and power plants in polluted background estimated by satellite observations, Atmos. Chem. Phys., 16, 5283–5298, doi:10.5194/acp-16-5283-2016, 2016.

Lu, Z., Streets, D., de Foy, B., Lamsal, L., Duncan, B., and Xing, J.: "Emissions of nitrogen oxides from US urban areas: estimation from Ozone Monitoring Instrument retrievals for 2005–2014", Atmos. Chem. Phys., 15, 10 367–10 383, doi:10.5194/acp-15-10367-2015, 2015.

Martin, R., Sauvage, B., Folkins, I., Sioris, C., Boone, C., Bernath, P., and Ziemke, J.: Space-based constraints on the production of nitric oxide by lightning, J. Geophys. Res., 112, doi:10.1029/2006JD007831, 2007.

McLinden, C. A., Fioletov, V., Boersma, K. F., Kharol, S. K., Krotkov, N., Lamsal, L., Makar, P. A., Martin, R. V., Veefkind, J. P., and Yang, K.: Improved satellite retrievals of NO_2 and SO_2 over the Canadian oil sands and comparisons with surface measurements, Atmospheric Chemistry and Physics, 14, 3637–3656, doi:10.5194/acp-14-3637-2014, 2014.

Mebust, A. and Cohen, R.: Observations of a seasonal cycle in NO_x emissions from fires in African woody savannas, Geophys. Res. Lett., 40, 1451–1455, doi:10.1002/grl.50343, 2013.

Mebust, A. and Cohen, R.: Space-based observations of fire NO_x emissions coefficients: a global biome-scale comparison, Atmos. Chem. Phys., 14, 2509–2524, doi:10.5194/acp-14-2509-2014, 2014.

Mebust, A. K., Russell, A. R., Hudman, R. C., Valin, L. C., and Cohen, R. C.: Characterization of wildfire NO_x emissions using MODIS fire radiative power and OMI tropospheric NO_2 columns, Atmos. Chem. and Phys., 11, 5839–5851, doi:10.5194/acp-11-5839-2011, 2011.

Miyazaki, K., Eskes, H., and Sudo, K.: Global NO_x emissions estimates derived from an assimilation of OMI tropospheric NO_2 columns, Atmos. Chem. Phys., 12, 2263–2288, doi:10.5194/acp-12-2263-2012, 2012.

Miyazaki, K., Eskes, H., Sudo, K., and Zhang, C.: Global lightning NO_x production estimated by an assimilation of multiple satellite data sets, Atmos. Chem. Phys., 14, 3277–3305, doi:10.5194/acp-14-3277-2014, 2014.

Nunnermacker, L. J., Imre, D., Daum, P. H., Kleinman, L., Lee, Y.-N., Lee, J. H., Springston, S. R., Newman, L., Weinstein-Lloyd, J., Luke, W. T., Banta, R., Alvarez, R., Senff, C., Sillman, S., Holdren, M., Keigley, G. W., and Zhou, X.: Characterization of the Nashville urban plume on July 3 and July 18, 1995, J. Geophys. Res. Atmos., 103, 28 129–28 148, doi:10.1029/98JD01961, 1998.

Palmer, P., Jacob, D., Chance, K., Martin, R., Spurr, R., Kurosu, T., Bey, I., Yantosca, R., Fiore, A., and Li, Q.: "Air mass factor formulation for spectroscopic measurements from satellites: Applications to formaldehyde retrievals from the Global Ozone Monitoring Experiment", J. Geophys. Res. Atmos., 106, 14 539–14 550, 2001.

Richter, A. and Wagner, T.: The Use of UV, Visible and Near IR Solar Back Scattered Radiation to Determine Trace Gases, in: The Remote Sensing of Tropospheric Composition from Space, edited by Burrows, J., Platt, U., and Borrell, P., Springer, New York, 2011.

Robere, R.: Interior Point Methods and Linear Programming, http://www.cs.toronto.edu/~robere/paper/interiorpoint.pdf, 2012.

Russell, A., Perring, A., Valin, L., Bucsela, E., Browne, E., Min, K., Wooldridge, P., and Cohen, R.: "A high spatial resolution retrieval of NO_2 column densities from OMI: method and evalutation", Atmos. Chem. Phys., 11, 8543–8554, doi:10.5194/acp-11-8543-2011, 2011.

Russell, A. R., Valin, L. C., and Cohen, R. C.: Trends in OMI NO_2 observations over the United States: effects of emission control technology and the economic recession, Atmospheric Chemistry and Physics, 12, 12 197–12 209, doi:10.5194/acp-12-12197-2012, 2012.

Schaap, M., Cuvelier, C., Hendriks, C., Bessagnet, B., Baldasano, J., Colette, A., Thunis, P., Karam, D., Fagerli, H., Graff, A., Kranenburg, R., Nyiri, A., Pay, M., Rouïl, L., Schulz, M., Simpson, D., Stern, R., Terrenoire, E., and Wind, P.: Performance of European chemistry transport models as function of horizontal resolution, Atmos. Environ., 112, 90–105, doi:http://dx.doi.org/10.1016/j.atmosenv.2015.04.003, 2015.

Schumann, U. and Huntrieser, H.: The global lightning-induced nitrogen oxides source, Atmos. Chem. Phys., 7, 3823–3907, 2007.

Spicer, C.: Nitrogen Oxide Reactions in the Urban Plume of Boston, Science, 215, 1095–1097, doi:10.1126/science.215.4536.1095, 1982.

Tong, D. Q., Lamsal, L., Pan, L., Ding, C., Kim, H., Lee, P., Chai, T., Pickering, K. E., and Stajner, I.: Long-term {NOx} trends over large cities in the United States during the great recession: Comparison of satellite retrievals, ground observations, and emission inventories, Atmospheric Environment, 107, 70–84, doi:http://dx.doi.org/10.1016/j.atmosenv.2015.01.035, 2015.

Travis, K. R., Jacob, D. J., Fisher, J. A., Kim, P. S., Marais, E. A., Zhu, L., Yu, K., Miller, C. C., Yantosca, R. M., Sulprizio, M. P., Thompson, A. M., Wennberg, P. O., Crounse, J. D., St. Clair, J. M., Cohen, R. C., Laugher, J. L., Dibb, J. E., Hall, S. R., Ullmann, K., Wolfe, G. M., Pollack, I. B., Peischl, J., Neuman, J. A., and Zhou, X.: NOx emissions, isoprene oxidation pathways, vertical mixing, and implications for surface ozone in the Southeast United States, Atmos. Chem. Phys. Discuss., 2016, 1–32, doi:10.5194/acp-2016-110, 2016.

United States Census Bureau: Annual Estimates of the Resident Population: April 1, 2010 to July 1, 2015. Metropolitan and Micropolitan Statistical Area; and for Puerto Rico., http://www.census.gov/popest/data/metro/totals/2015/index.html.

Valin, L., Russell, A., Hudman, R., and Cohen, R.: Effects of model resolution on the interpretation of satellite NO_2 observations, Atmos. Chem. Phys., 11, 11 647–11 655, doi:10.5194/acp-11-11647-2011, 2011.

Valin, L., Russell, A., and Cohen, R.: "Variations of OH radical in an urban plume inferred from NO_2 column measurements", Geophys. Res. Lett., 40, 1856–1860, doi:10.1002/grl.50267, 2013.

Veefkind, J., Aben, I., McMullan, K., Förster, H., de Vries, J., Otter, G., Claas, J., Eskes, H., de Haan, J., Kleipool, Q., van Weele, M., Hasekamp, O., Hoogeveen, R., Landgraf, J., Snel, R., Tol, P., Ingmann, P., Voors, R., Kruizinga, B., Vink, R., Visser, H., and Levelt, P.: TROPOMI on the ESA Sentinel-5 Precursor: A GMES mission for global observations of the atmospheric composition for climate, air quality and ozone layer applications, Remote Sens. Environ., 120, 70–83, doi:http://dx.doi.org/10.1016/j.rse.2011.09.027, 2012.

Wild, O. and Prather, M. J.: Global tropospheric ozone modeling: Quantifying errors due to grid resolution, J. Geophys. Res. Atmos., 111, D11 305, doi:10.1029/2005JD006605, 2006.

Wright, M.: The interior-point revolution in optimization: History, recent developments, and lasting consequences, Bull. Amer. Math. Soc., 42, 39–56, http://www.ams.org/journals/bull/2005-42-01/S0273-0979-04-01040-7/, 2005.

Yamaji, K., Ikeda, K., Irie, H., Kurokawa, J.-i., and Ohara, T.: Influence of model-grid resolution on NO_2 vertical column densities over East Asia, J. Air. Waste. Manage., 64, 436–444, doi:10.1080/10962247.2013.827603, 2014.

Zare, A.: in prep.

Ziemke, J., Chandra, S., and Bhartia, P.: "Cloud slicing: A new technique to derive upper tropospheric ozone from satellite measurements", J. Geophys. Res. Atmos., 106, 9853–9867, 2001.

Atmos. Chem. Phys. Discuss., doi:10.5194/acp-2016-536, 2016
Manuscript under review for journal Atmos. Chem. Phys.
Published: 12 July 2016

Atmospheric Chemistry and Physics Discussions

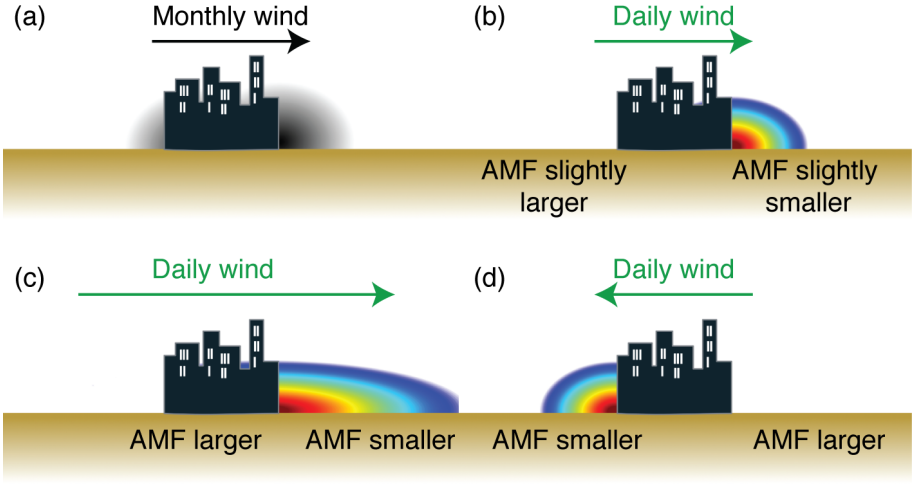

Figure 1. An illustration of the central issues that will be discussed in this paper. (a) The monthly average a priori profiles, shown as the grayscale plumes. (b) A case when the daily wind is similar to the monthly average wind. (c) A case where the daily wind is significantly faster than average, but blows in the same direction. (d) A case where the daily wind direction is different than average. The text below each panel describes how the AMF derived from the daily profile would compare with those derived from the monthly a priori.

Atmos. Chem. Phys. Discuss., doi:10.5194/acp-2016-536, 2016
Manuscript under review for journal Atmos. Chem. Phys.
Published: 12 July 2016

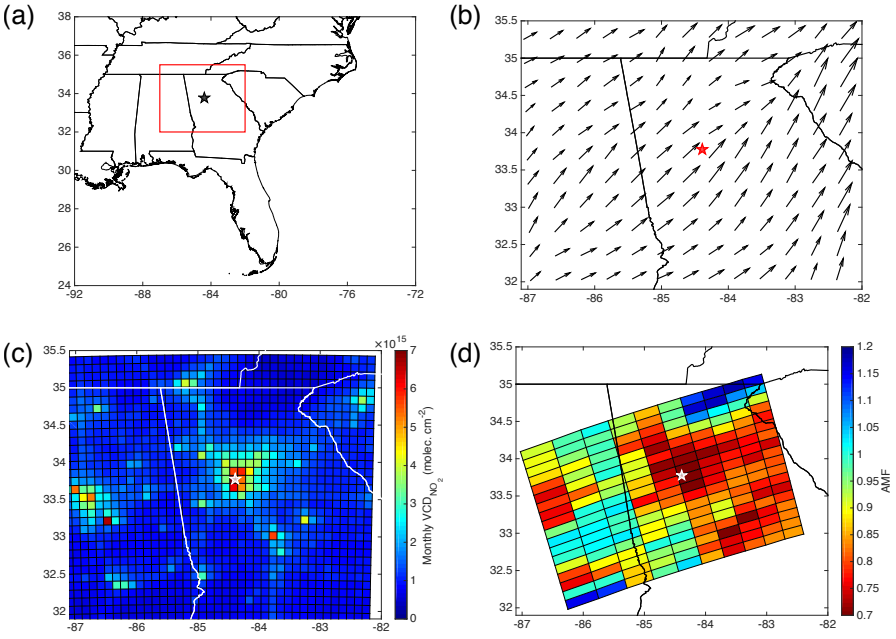

Figure 2. Average conditions for 1 June–30 Aug, 2013. (a) The red box indicates the part of the SE US being considered. (b) Surface wind directions from the WRF model. (c) WRF-Chem tropospheric NO_2 columns. (d) AMFs for the pseudo-retrieval calculated using the average monthly NO_2 a priori. The direction of the colorbar is reversed in (d), as small AMFs correspond to high modeled VCDs. In all panels, the star (★) indicates the position of Atlanta. Longitude and latitude are marked on the x- and y- axes, respectively.

Atmos. Chem. Phys. Discuss., doi:10.5194/acp-2016-536, 2016
Manuscript under review for journal Atmos. Chem. Phys.
Published: 12 July 2016

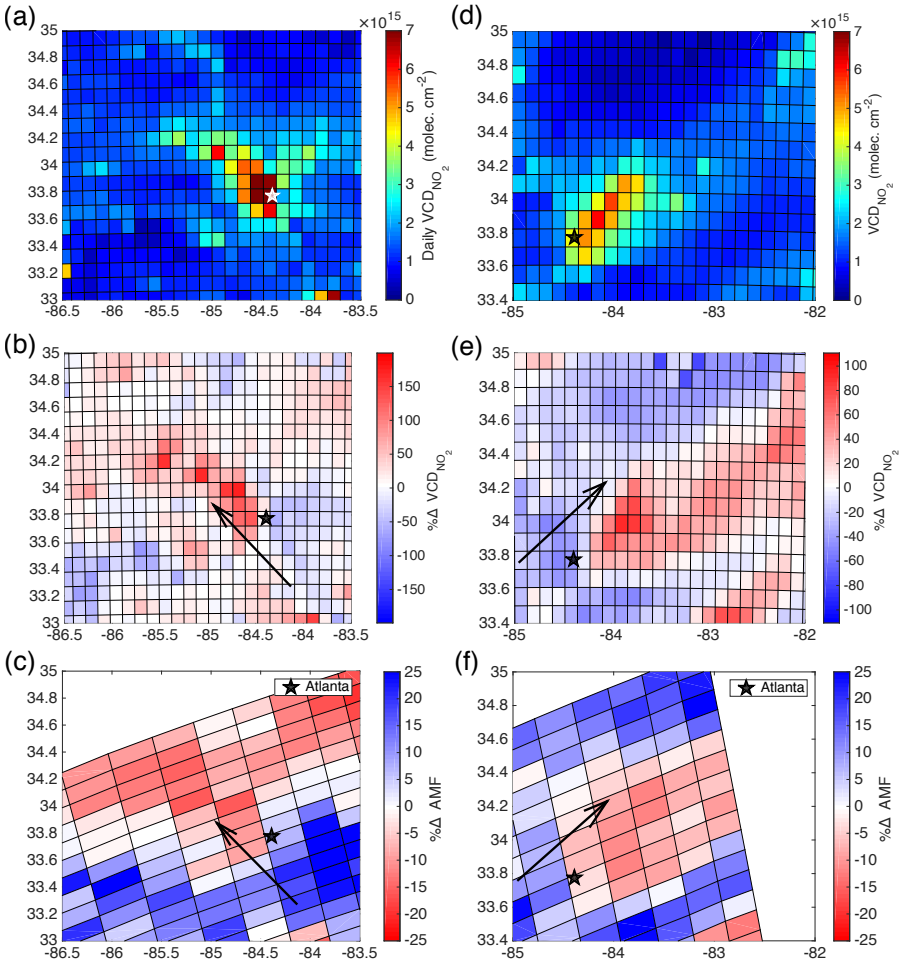

Figure 3. Results from 22 June (a–c) and 18 June (d–f). (a,d) WRF-Chem tropospheric NO_2 columns for 1900 UTC. (b,e) The percent difference in WRF-Chem tropospheric NO_2 columns at 1900 UTC for that day vs. the monthly average. (c,f) Percent difference in AMFs using hybrid daily profiles vs. the monthly average profiles in the pseudo-retrieval. In all panels, the star (★) indicates the position of Atlanta, and the wind direction around Atlanta is shown by the arrow in the lower four panels. Longitude and latitude are marked on the x- and y-axes, respectively.

Atmos. Chem. Phys. Discuss., doi:10.5194/acp-2016-536, 2016
Manuscript under review for journal Atmos. Chem. Phys.
Published: 12 July 2016

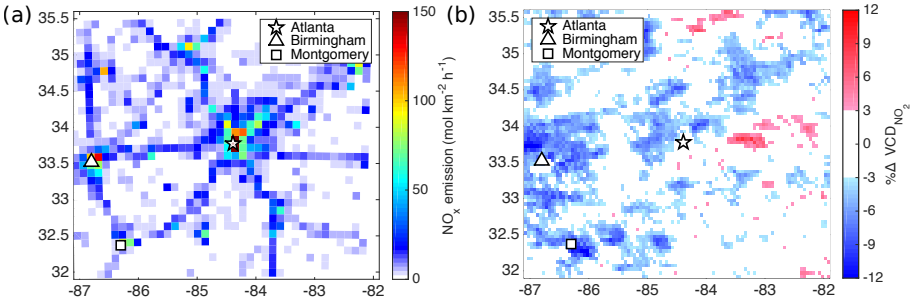

Figure 4. (a) NO emissions from WRF-Chem at 12 km resolution. (b) The change in retrieved VCDs averaged over 1 June to 30 Aug. Pixels with a cloud fraction $> 20\%$ or that are affected by the row anomaly are excluded from the average. The color scale is reversed from Fig. 3c,f to reflect the inverse relationship between VCD and AMF. Longitude and latitude are marked on the x- and y- axes, respectively.

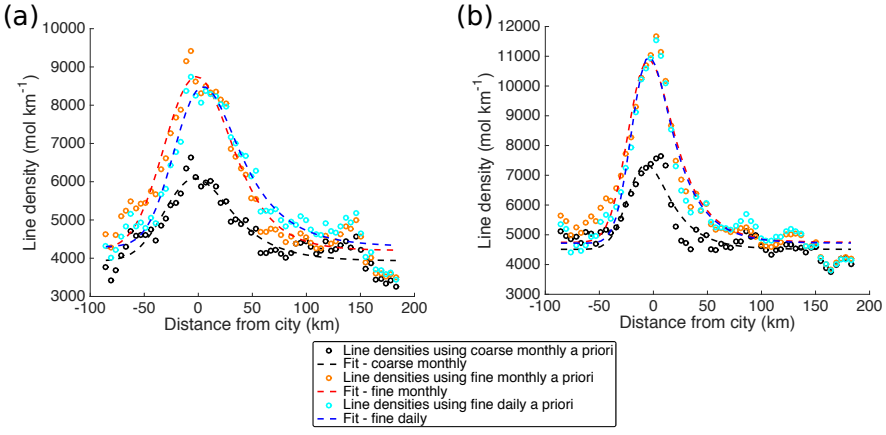

Figure 5. Line densities around Atlanta, GA averaged over the study period when using monthly average and daily a priori (open circles), and the corresponding fits of exponentially-modified Gaussian functions (dashed lines). Black series are derived from a retrieval using a monthly average a priori at 108 km resolution; red series from a monthly average a priori at 12 km resolution, and blue from the daily profiles at 12 km resolution. (a) Average of days with wind speed ≥ 3.0 m/s. (b) Average of days with wind speed < 3.0 m/s.

Atmos. Chem. Phys. Discuss., doi:10.5194/acp-2016-536, 2016
Manuscript under review for journal Atmos. Chem. Phys.
Published: 12 July 2016

Atmospheric Chemistry and Physics Discussions

Parameter	Physical significance	Lower Bound	Upper Bound	Best guess initial value
a (mol)	NO_2 burden	0	∞	$\int_{x_{\min}}^{x_{\max}} \mathrm{NO_2}(x)\, dx$
x_0 (km)	Distance traveled in 1 lifetime	1.6	∞	54
μ_x (km)	Emission center	$\min(x)$	$\max(x)$	$x_{\max(\mathrm{NO2})}$
σ_x (km)	Gaussian smoothing	2.5	$x_{\max(\mathrm{NO2})} - \min(x)$	FWHM / 2.355
B (mol)	Background	0	$\max(\mathrm{NO_2})$	$\min(\mathrm{NO_2})$
Additional constraints				
$\mu_x + x_0 \leq \max(x)$				
$\exp\left(\frac{\mu_x}{x_0} + \frac{\sigma_x^2}{2x_0^2} - \frac{x}{x_0}\right) \leq 20$				

Table 1. Constraints imposed on the solutions permitted to fmincon, in the form of upper and lower bounds, with additional linear and nonlinear constraints. x refers to the x-coordinates associated with the data, i.e. distance from the city center. $x_{\max(\mathrm{NO2})}$ indicates the x coordinate where the greatest NO_2 line density is present. NO_2 refers to the values of the line density. FWHM is the full width at half maximum of the Gaussian. For additional discussion of the reasoning for the selection of these values, see the supplement.

Atmos. Chem. Phys. Discuss., doi:10.5194/acp-2016-536, 2016
Manuscript under review for journal Atmos. Chem. Phys.
Published: 12 July 2016

Atmospheric Chemistry and Physics Discussions

	Percent of days with ΔVCD $> 1 \times 10^{15}$ molec. cm^{-2}	Min. change (molec. cm^{-2})	Max. change (molec. cm^{-2})
Atlanta	43%	-2.0×10^{15}	$+2.0 \times 10^{15}$
Birmingham	59%	-3.9×10^{15}	$+3.7 \times 10^{15}$
Montgomery	27%	-2.1×10^{15}	$+2.3 \times 10^{15}$

Table 2. Statistics on the frequency and magnitude of changes in the retrieved VCDs using a daily vs. monthly average profile for pixels with centers within 50 km of Atlanta, GA (84.39° W, 33.775° N), Birmingham, AL (86.80° W, 33.52° N) and Montgomery, AL (86.30° W, 32.37° N). The "percent of days" values are calculated as the number of days with at least one pixel in that subset with a change $> 1 \times 10^{15}$ molec. cm^{-2} divided by the number of days with at least one pixel unobscured by clouds or the row anomaly.

Atmos. Chem. Phys. Discuss., doi:10.5194/acp-2016-536, 2016
Manuscript under review for journal Atmos. Chem. Phys.
Published: 12 July 2016

Atmospheric Chemistry and Physics Discussions

		Wind ≥ 3.0 m/s			Wind < 3.0 m/s		
		Monthly 108 km	Monthly 12 km	Daily 12 km	Monthly 108 km	Monthly 12 km	Daily 12 km
Atlanta	a (mol NO_2)	$1.8 \pm 0.7 \times 10^5$	$4. \pm 2 \times 10^5$	$3. \pm 1 \times 10^5$	$1.5 \pm 0.6 \times 10^5$	$4. \pm 1 \times 10^5$	$3. \pm 1 \times 10^5$
	x_0 (km)	32 ± 13	26 ± 11	34 ± 14	23 ± 10	24 ± 10	24 ± 10
	μ_x (km)	$-23. \pm 9$	$-20. \pm 8$	$-15. \pm 6$	$-20. \pm 8$	$-18. \pm 7$	$-17. \pm 7$
	σ_x (km)	$23. \pm 9$	30 ± 10	$22. \pm 9$	$14. \pm 6$	$15. \pm 6$	$13. \pm 5$
	B (mol NO_2 km^{-1})	$4. \pm 2 \times 10^3$	$4. \pm 2 \times 10^3$	$4. \pm 2 \times 10^3$	$5. \pm 2 \times 10^3$	$5. \pm 2 \times 10^3$	$5. \pm 2 \times 10^3$
Birmingham	a (mol NO_2)	$1.6 \pm 0.5 \times 10^5$	$3. \pm 1 \times 10^5$	$4. \pm 1 \times 10^5$	$4. \pm 1 \times 10^5$	$3. \pm 1 \times 10^5$	$4. \pm 1 \times 10^5$
	x_0 (km)	50 ± 20	30 ± 10	50 ± 20	220 ± 80	40 ± 10	70 ± 20
	μ_x (km)	$-21. \pm 7$	$-25. \pm 8$	$-15. \pm 5$	-50 ± 20	$-27. \pm 9$	$-26. \pm 9$
	σ_x (km)	$24. \pm 8$	$27. \pm 9$	$23. \pm 8$	$21. \pm 7$	$25. \pm 8$	$22. \pm 8$
	B (mol NO_2 km^{-1})	$4. \pm 1 \times 10^3$	$4. \pm 1 \times 10^3$	$4. \pm 1 \times 10^3$	$4. \pm 1 \times 10^3$	$5. \pm 2 \times 10^3$	$5. \pm 2 \times 10^3$

Table 3. Values of the five fitting parameters for the EMG functions (Eq. 8) used to fit the distributions of line densities around Atlanta and Birmingham. a represents the total NO_x burden, x_0 is the distance the plume travels in one lifetime, μ_x is the center of emissions relative to the city center, σ_x describes the Gaussian smoothing, and B the background line density.

Atmos. Chem. Phys. Discuss., doi:10.5194/acp-2016-536, 2016
Manuscript under review for journal Atmos. Chem. Phys.
Published: 12 July 2016

Atmospheric Chemistry and Physics Discussions

		Atlanta			Birmingham		
	Wind speed bin	Monthly 108 km	Monthly 12 km	Daily 12 km	Monthly 108 km	Monthly 12 km	Daily 12 km
E (Mg NO_x h^{-1})	WRF-Chem NEI		**13.74**			**10.49**	
	≥ 3.0	$6. \pm 4$	$16. \pm 9$	$11. \pm 7$	$4. \pm 2$	$10. \pm 5$	$8. \pm 4$
	≥ 4.0	$6. \pm 3$	20 ± 10	$11. \pm 6$	$4. \pm 2$	$13. \pm 6$	$9. \pm 4$
	≥ 5.0	-	-	-	$6. \pm 3$	$15. \pm 9$	$11. \pm 6$
τ (h)	≥ 3.0	1.6 ± 0.7	1.3 ± 0.5	1.7 ± 0.7	2.5 ± 0.9	1.8 ± 0.6	2.6 ± 0.9
	≥ 4.0	1.8 ± 0.7	1.2 ± 0.5	1.8 ± 0.8	2.2 ± 0.8	1.5 ± 0.5	2.2 ± 0.8
	≥ 5.0	-	-	-	1.8 ± 0.7	1.3 ± 0.5	1.8 ± 0.7

Table 4. Values of the emission rates (E) and effective lifetime (τ) obtained when the separation between slow and fast winds is set at 3, 4, and 5 m s^{-1}. For comparison, the total NO_x emission for all 12 km WRF-Chem grid cells within 50 km of each city is given. These emissions are derived from NEI 11 and scaled to 88.9% to account for 2011–2013 reductions. Uncertainties calculated as described in the supplement.